Electronic Supplementary Information

Poly(2,6-anthraquinonyl disulfide) as a high-capacity and high-power cathode for rechargeable magnesium batteries: Extra capacity provided by the disulfide group

Xin Ren[a], Donggang Tao[a], Yudi Tang[a], Yuliang Cao[b], Fei Xu*[a]

[a] Key Laboratory of Hydraulic Machinery Transients, Ministry of Education, School of Power and Mechanical Engineering, Wuhan University, Wuhan 430072, China.

[b] Hubei Key Lab of Electrochemical Power Sources, College of Chemistry & Molecular Science, Wuhan University, Wuhan 430072, China.

* E-mail: Fei Xu (xufei2058@whu.edu.cn)

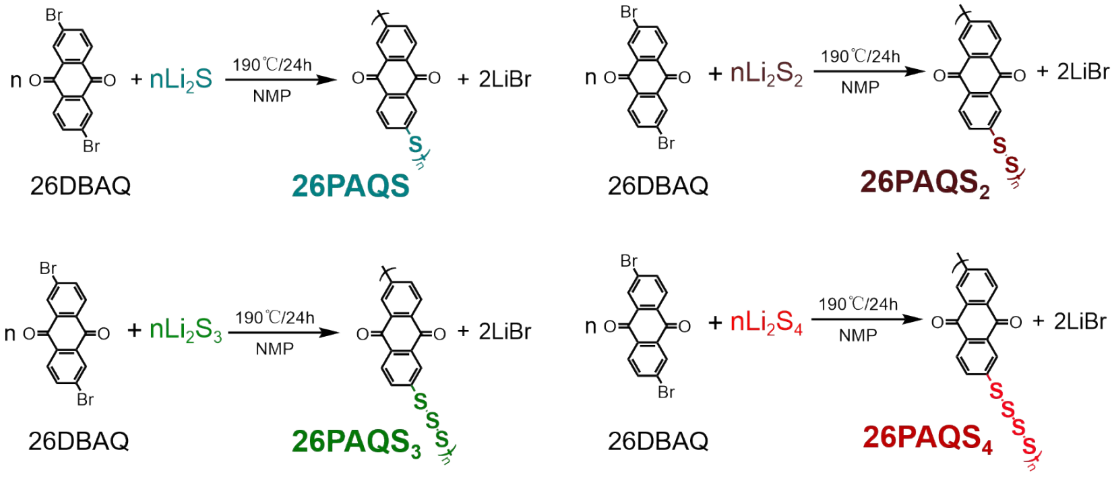

Fig. S1 Proposed synthesis routines.

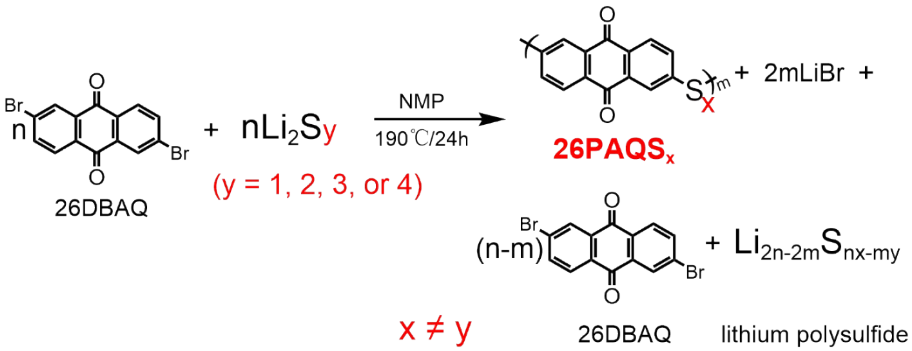

Fig. S2 Actual synthesis routines.

Fig. S1 describes the proposed synthesis routines. However, the actual reactions are different from Fig. S1, because the nucleophilicity of S_y^{2-} decreases with the increasing y value (Fig. S2). This is reflected in the decreasing yields (Table S1). The unreacted 26DBAQ and remaining lithium polysulfide (Fig. S2) existed in the liquid solution and were seperated from the solid products ($26PAQS_x$). This would lead to a difference of the sulfur contents between the starting materials (y of Li_2S_y in Fig. S2) and the products (x of $26PAQS_x$ in Fig. S2). The actual sulfur contents of the products were determined by EDS and ICP and shown in Fig. 1b of the main text.

Table S1 Yields of 26PAQS, $26PAQS_{1.4}$, $26PAQS_{1.9}$ and $26PAQS_{2.2}$.

Samples	Yields
26PAQS	64
$26PAQS_{1.4}$	52
$26PAQS_{1.9}$	35
$26PAQS_{2.2}$	20

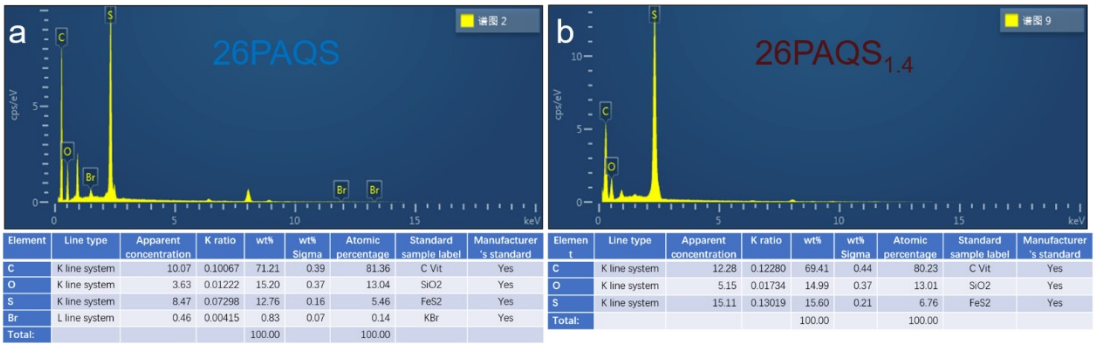

Element	Line type	Apparent concentration	K ratio	wt%	wt% Sigma	Atomic percentage	Standard sample label	Manufacturer 's standard
C	K line system	10.07	0.10067	71.21	0.39	81.36	C Vit	Yes
O	K line system	3.63	0.01222	15.20	0.37	13.04	SiO2	Yes
S	K line system	8.47	0.07298	12.76	0.16	5.46	FeS2	Yes
Br	L line system	0.46	0.00415	0.83	0.07	0.14	KBr	Yes
Total:				100.00		100.00		

Element	Line type	Apparent concentration	K ratio	wt%	wt% Sigma	Atomic percentage	Standard sample label	Manufacturer 's standard
C	K line system	12.28	0.12280	69.41	0.44	80.23	C Vit	Yes
O	K line system	5.15	0.01734	14.99	0.37	13.01	SiO2	Yes
S	K line system	15.11	0.13019	15.60	0.21	6.76	FeS2	Yes
Total:				100.00		100.00		

Element	Line type	Apparent concentration	K ratio	wt%	wt% Sigma	Atomic percentage	Standard sample label	Manufacturer 's standard
C	K line system	3.72	0.03716	69.11	0.81	81.32	C Vit	Yes
O	K line system	1.39	0.00466	11.44	0.59	10.11	SiO2	Yes
S	K line system	6.94	0.05980	19.44	0.48	8.57	FeS2	Yes
Total:				100.00		100.00		

Element	Line type	Apparent concentration	K ratio	wt%	wt% Sigma	Atomic percentage	Standard sample label	Manufacturer 's standard
C	K line system	1.84	0.01837	64.24	1.23	79.04	C Vit	Yes
O	K line system	0.86	0.00290	10.85	0.72	10.03	SiO2	Yes
S	K line system	5.19	0.04473	22.94	0.77	10.57	FeS2	Yes
Br	L line system	0.38	0.00345	1.97	0.18	0.36	KBr	Yes
Total:				100.00		100.00		

Fig. S3 EDS of (a) 26PAQS, (b) 26PAQS$_{1.4}$, (c) 26PAQS$_{1.9}$ and (d) 26PAQS$_{2.2}$.

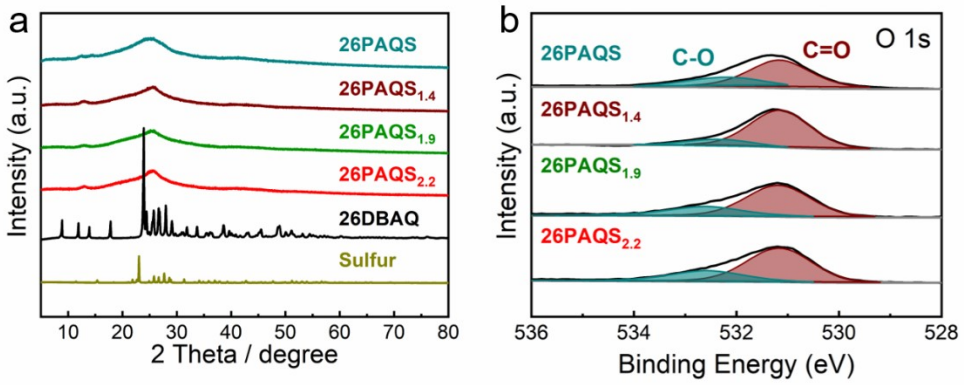

Fig. S4 (a) XRD patterns and (b) O1s XPS spectra of 26PAQS, 26PAQS$_{1.4}$, 26PAQS$_{1.9}$, 26PAQS$_{2.2}$ and 26DBAQ.

The C=O (287.1 eV)/C–O (285.5 eV)/C–C (284.8 eV) peaks in the C 1s spectra and the C–O (533.1 eV)/C=O (531.1 eV) peaks in the O 1s spectra verify that the conjugated carbonyl group remains stable during the polymerization.

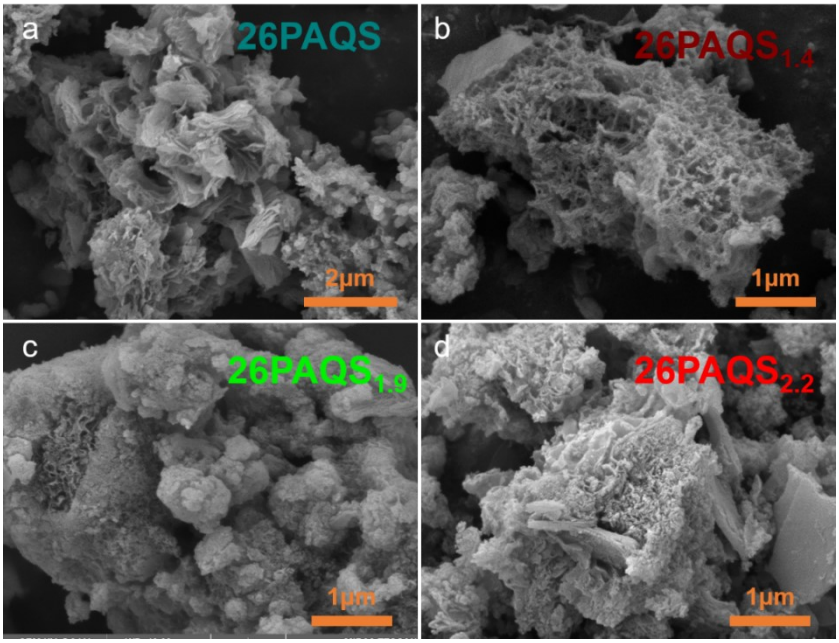

Fig. S5 SEM images of (a) 26PAQS, (b) $26PAQS_{1.4}$, (c) $26PAQS_{1.9}$ and (d) $26PAQS_{2.2}$.

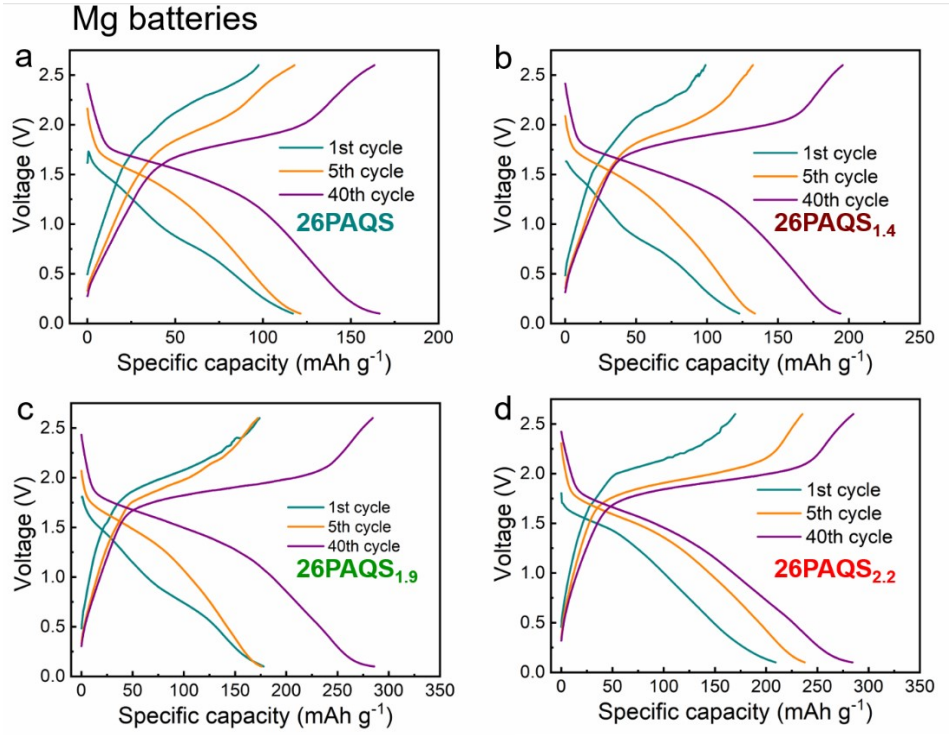

Fig. S6 Charge/discharge profiles of (a) 26PAQS, (b) $26PAQS_{1.4}$, (c) $26PAQS_{1.9}$ and (d) $26PAQS_{2.2}$ at 50 mA g^{-1}.

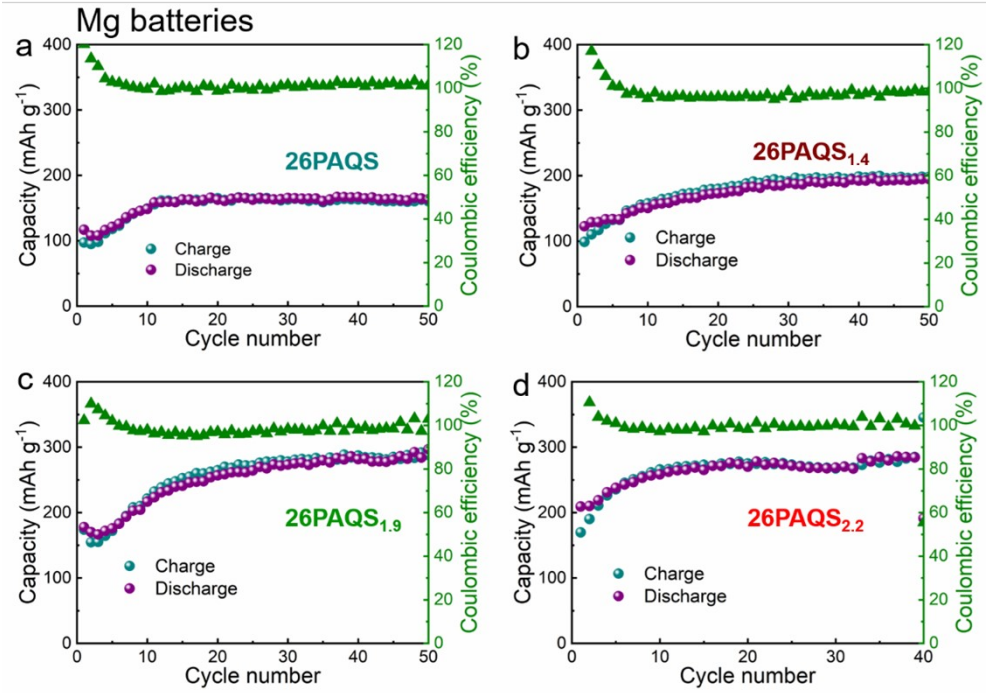

Fig. S7 Cycling performances of (a) 26PAQS, (b) $26PAQS_{1.4}$, (c) $26PAQS_{1.9}$ and (d) $26PAQS_{2.2}$ at 50 mA g^{-1}.

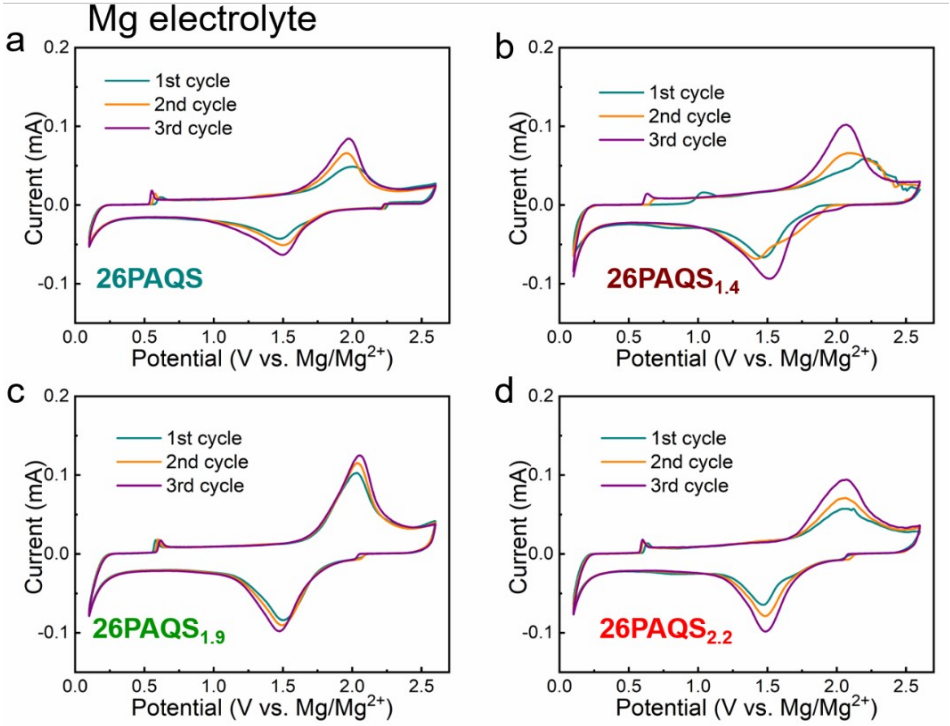

Fig. S8 CV curves of (a) 26PAQS, (b) $26PAQS_{1.4}$, (c) $26PAQS_{1.9}$ and (d) $26PAQS_{2.2}$ in Mg electrolytes at first three cycles (0.1 mV s^{-1}).

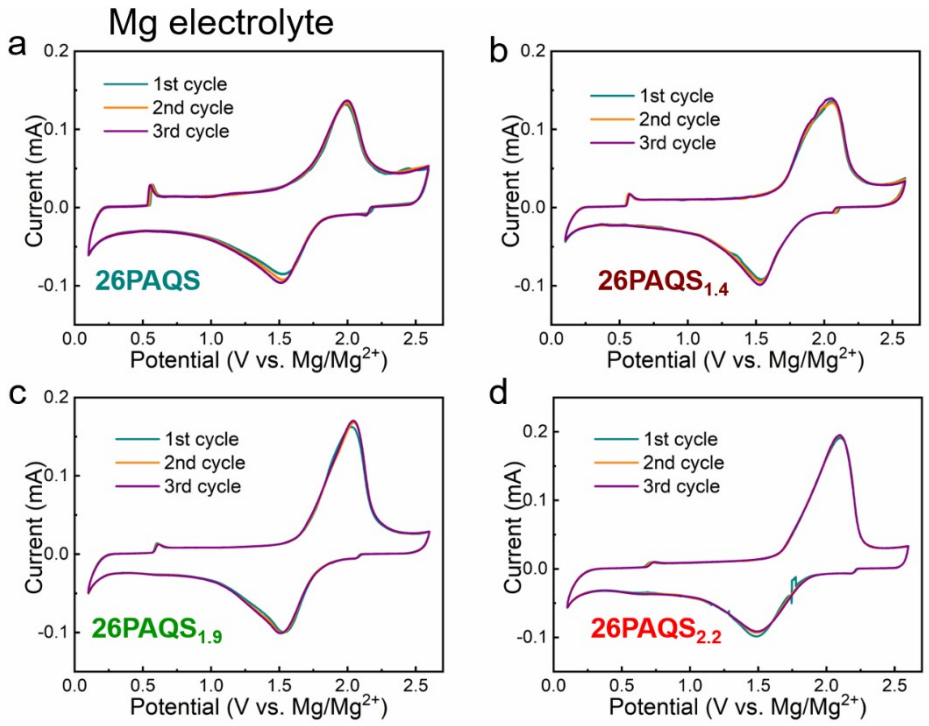

Fig. S9 CV curves of (a) 26PAQS, (b) $26PAQS_{1.4}$, (c) $26PAQS_{1.9}$ and (d) $26PAQS_{2.2}$ in Mg electrolytes after activations (0.1 mV s^{-1}).

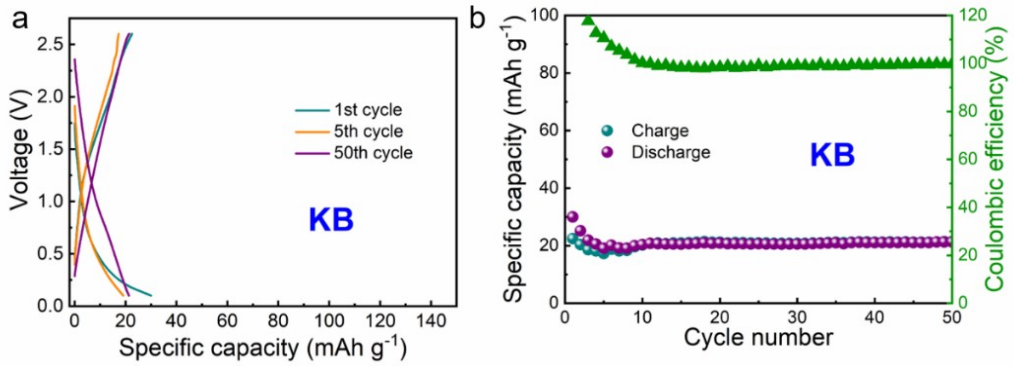

Fig. S10 (a) Charge/discharge curves and (b) cycling performance of KB. The mass of KB was the same as that contained in the $26PAQS_x$ cathodes, and the mass of the active material was set the same as the $26PAQS_x$ electrode for a comparison.

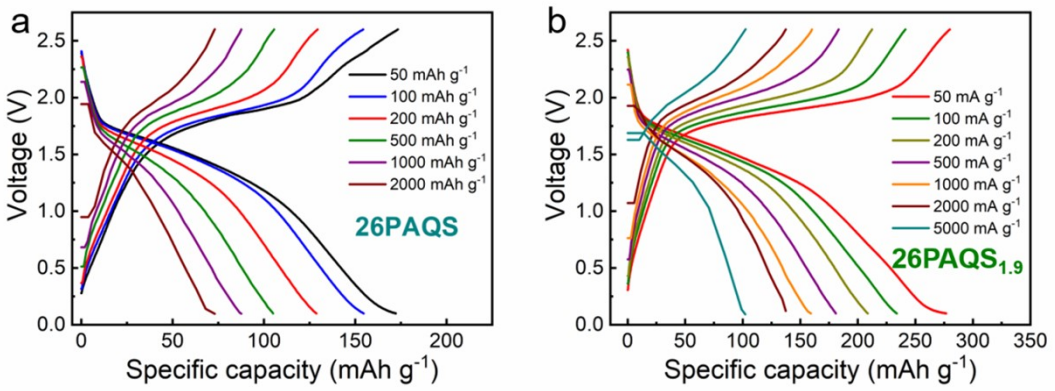

Fig. S11 Charge/discharge profiles of (a) 26PAQS and (b) $26PAQS_{1.9}$ at different current densities.

Table S2 Energy density calculation of rechargeable Mg batteries.

Cathodes	Electrolytes	Cc (mAh g^{-1})	Ca (mAh g^{-1})	C (wt%)	Ce (mAh g^{-1})	E (V)	Specific Energy (Wh kg^{-1})
Mo_6S_8[1]	$(PhMgCl)_2$-$AlCl_3$/THF	76	2205	0.1041	40.88	1.10	28.9
Mo_6Se_8[2]	$(PhMgCl)_2$-$AlCl_3$/THF	80	2205			1.05	28.1
DMBQ[3]	$Mg(TFSI)_2$-$2MgCl_2$ /DME	225	2205	0.07767	43.82	2.00	72.2
PHV-Cl[4]	$(PhMgCl)_2$-$AlCl_3$/THF	171	2205	0.1041	40.88	1.30	42.3
NP[5]	$Mg(TFSI)_2$-$MgCl_2$ /TEGDME-DOL	70	2205	0.0291	16.42	1.60	21.2
Mg-14PAQ[6]	$Mg(HMDS)_2$-$4MgCl_2$ /THF	133	2205	0.1032	58.23	1.38	54.6
P(NDI2OD-T2)[7]	$Mg(TFSI)_2$/diglyme	54	2205	/	/	1.42	74.8
Mg-P14AQ[7]	$Mg(TFSI)_2$/diglyme	193	2205	/	/	1.37	243.1
COF[8]	$Mg(TFSI)_2$/DME	114	2205	/	/	1.35	146.4
$Cu_{2-x}Se$[9]	$Mg(HMDS)_2$-$2AlCl_3$ /diglyme	214	2205	/	/	1.00	195.1
E-VS_2[10]	$(PhMgCl)_2$-$AlCl_3$/THF	237	2205	0.1041	40.88	1.03	34.3
GO-V_2O_5[11]	$Mg(AlCl2BuEt)_2$-THF	180	2205	0.0992	13.56	1.50	18.8
$Mg_{0.21}Ti_3C_2T_x$[12]	$(PhMgCl)_2$-$AlCl_3$/THF	210	2205	0.0562	22.08	1.50	29.7
PA-$VOPO_4$[13]	$(PhMgCl)_2$-$AlCl_3$/THF	275	2205	0.0690	27.08	1.00	24.4
PEO-MoS_2[14]	$(PhMgCl)_2$-$AlCl_3$/THF	70	2205	0.1037	40.74	0.70	17.8
TiS_2[15]	$(PhMgCl)_2$-$AlCl_3$/THF	160	2205	0.1041	40.88	0.90	28.9
VS4@Ti_3C_2/C[16]	$(PhMgCl)_2$-$AlCl_3$/THF	490	2205	0.0690	27.08	1.00	25.4
26PAQS$_{1.9}$	$Mg(TFSI)_2$-$2MgCl_2$/DME	276	2205	/	/	1.51	367.9

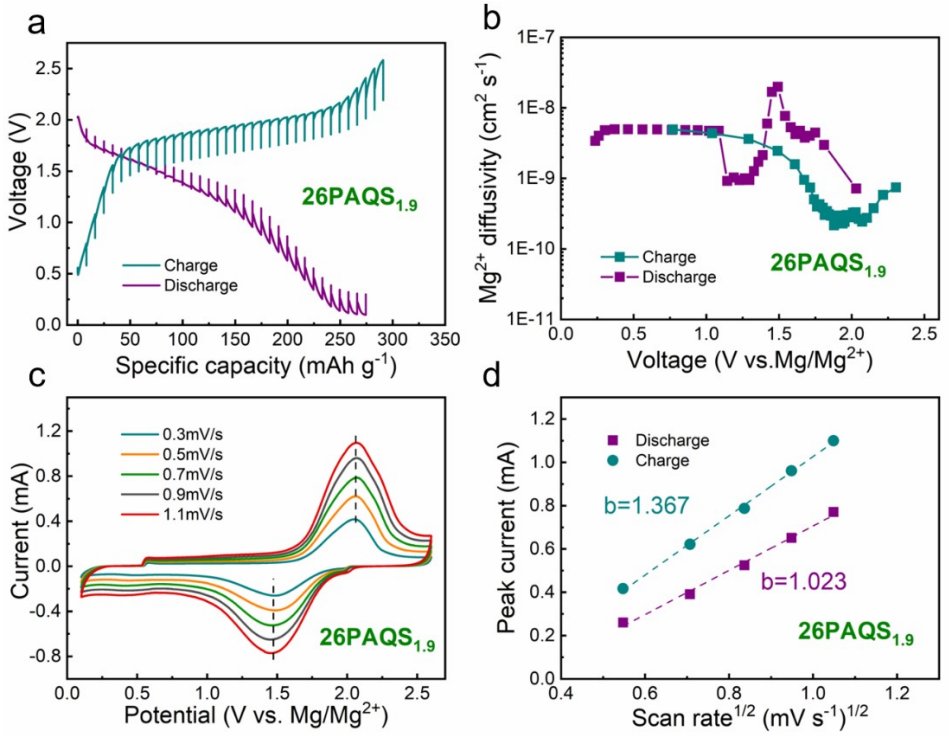

Fig. S12 (a) GITT profiles and (b) Mg^{2+} diffusion coefficients of $26PAQS_{1.9}$. (c) CV curves of $PAQS_{1.9}$ at different scan rates. (d) i_p vs. $-v^{1/2}$ plots for the redox peaks of $PAQS_{1.9}$.

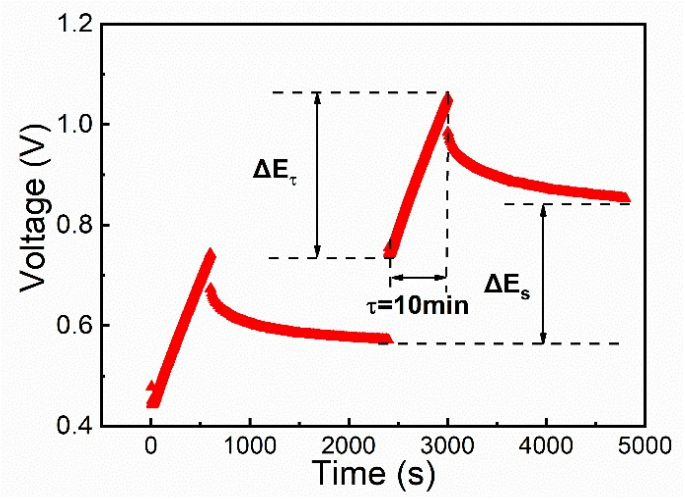

Fig. S13 Calculation details of GITT.

The Mg^{2+} diffusivity can be calculated via the following formula:

$$D^{GITT} = \frac{4}{\pi\tau}\left(\frac{m_B V_M}{M_B S}\right)^2\left(\frac{\triangle E_s}{\triangle E_\tau}\right)^2$$

Where τ refers to constant current pulse time, m_B and M_B are the mass, molar mass of the cathode material, respectively. V_m is the molar volume of the compound and S is the area of electrode-electrolyte interface. ΔE_S is voltage difference during a single-step experiment, and ΔE_τ is the total change of cell voltage during a constant current pulse.

Table S3 Calculation of Mg^{2+} diffusion coefficients at 1.1 mV s^{-1}.

	26PAQS$_{1.9}$	
	$i_p/v^{1/2}$	D (cm^2 s^{-1})
Discharge	1.023	6.80×10^{-9}
charge	1.367	1.21×10^{-8}

The diffusion coefficient of Mg^{2+} is calculated by the following Randles-Sevcik Equation:

$$\boldsymbol{i_p = 2.69\times10^5 n^{3/2} A D^{1/2} v^{1/2} C_0}$$

where i_p is the peak current (A), n is the number of electrons per molecule during the reaction, A is the contact area between the electrode and electrolyte , D is the diffusion coefficient of Mg^{2+} (cm^2 s^{-1}), C_0 is the concentration of Mg^{2+} ion in the electrode material, and v is the scan rate (V s^{-1}).

Calculation of specific energy for rechargeable Mg batteries: [8]

For energy density calculation of Mg batteries without considering electrolyte mass, the calculation is based on the following equations:

$$E_S = E/(C_c^{-1} + C_a^{-1})$$

where E is the average discharge voltage, C_c is specific capacity of cathode, C_a is specific capacity of anode.

Reference

[1] P. Saha, P. H. Jampani, M. K. Datta, C. U. Okoli, A. Manivannan, P. N. Kumta, *J. Electrochem. Soc.* 2014, *161*, A593–A598.

[2] P. Saha, P. H. Jampani, M. K. Datta, D. Hong, B. Gattu, P. Patel, K. S. Kadakia, A. Manivannan, P. N. Kumta, *Nano Res.* 2017, *10* (12), 4415–4435.

[3] B. Pan, D. Zhou, J. Huang, L. Zhang, A. K. Burrell, J. T. Vaughey, Z. Zhang, C. Liao, *J. Electrochem. Soc.* 2016, *163,* A580–A583.

[4] A. B. Ikhe, N. Naveen, K. Sohn, M. Pyo, *Electrochim. Acta* 2018, *283,* 393–400.

[5] T. Bančič, J. Bitenc, K. Pirnat, A. K. Lautar, J. Grdadolnik, A. R. Vitanova, R. Dominko, *J. Power Sources* 2018, *395*, 25–30.

[6] B. Pan, J. Huang, Z. Feng,; L. Zeng, M. He, L. Zhang, J. T. Vaughey, M. J. Bedzyk, P. Fenter, Z. Zhang, A. K. Burrell, C. Liao, *Adv. Energy Mater.* 2016, *6*, 1600140.

[7] H. Dong, Y. Liang, O. Tutusaus, R. Mohtadi, Y. Zhang, F. Hao, Y. Yao, *Joule* 2019, *3*, 782–793.

[8] R. Sun, S. Hou, C. Luo, X. Ji, L. Wang, L. Mai, C. Wang, *Nano Lett.* 2020, *20*, 3880–3888.

[9] X. Xue, R. Chen, X. Song, A. Tao, W. Yan, W. Kong, Z. Jin, *Adv. Funct. Mater.* 2021, *31*, 2009394.

[10] P. Jing, H. Lu, W. Yang, Y. Cao, *Electrochimica Acta* 2020, *330*, 135263.

[11] X. Du, G. Huang, Y. Qin, L. Wang, *RSC Adv.* 2015, *5*, 76352–76355.

[12] M. Q. Zhao, C. E. Ren, M. Alhabeb, B. Anasori, M. W. Barsoum, Y. Gogotsi, *ACS Appl. Energy Mater.* 2019, *2*, 1572−1578.

[13] L. Zhou, Q. Liu, Z. Zhang, K. Zhang, F. Xiong, S. Tan, Q. An, Y. M. Kang, Z. Zhou, L. Mai, *Adv. Mater.* 2018, *30*, 1801984.

[14] H. J. Lee, J. Shin, J. W. Choi, *Adv. Mater.* 2018, *30,* 1705851.

[15] X. Sun, P. Bonnick, L. F. Nazar, *ACS Energy Lett.* 2016, *1*, 297–301.

[16] J. Zhu, X. Zhang, H. Gao, Y. Shao, Y. Liu, Y. Zhu, J. Zhang, L. Li, *Journal of Power Sources* 2022, *518*, 230731.